Articles

Preparation and Electrical Properties of Manganese-incorporated Neodymium Oxide System

Jong Sik Park, Keu Hong Kim, Chul Hyun Yo, and Sung Han Lee*

Department of Chemistry, Yonsei University, Wonju 222-701, Korea

Received March 4, 1994

Manganese-incorporated neodymium oxide systems with a variety of Mn mol% were prepared to investigate the effect of doping on the electrical properties of neodymium oxide. XRD, XPS, SEM, DSC, and TG techniques were used to analyze the specimens. The systems containing 2, 5, 8, and 10 mol% Mn were found to be solid solutions by X-ray diffraction analysis and the lattice parameters were obtained for the single-phase hexagonal structure by the Nelson-Riley method. The lattice parameters, *a* and *c*, decreased with increasing Mn mol%. Scanning electron photomicrographs of the specimens showed that the grain size decreased with increasing Mn mol%. The curves of log conductivity plotted as a function of 1/T in the temperature range from 500 to 1000℃ at Po_2's of 10^{-5} to 10^{-1} atm for the specimens were divided into high- and low-temperature regions with inflection points near 820-890℃. The activation energies obtained from the slopes were 0.53-0.87 eV for low-temperature region and 1.40-1.91 eV for high-temperature region. The electrical conductivities increased with increasing Mn mol% and Po_2, indicating that all the specimens were *p*-type semiconductors. At Po_2's below 10^{-3} atm, the electrical conductivity was affected by the chemisorption of oxygen molecule in the temperature range of 660 to 850℃. It is suggested that electron holes generated by oxygen incorporation into the oxide are charge carriers for the electrical conduction in the high-temperature region and the system includes ionic conduction owing to the diffusion of oxygen atoms in the low-temperature region.

Introduction

Rare earth metal oxides containing two or three cations have attracted increased attention for applications in photocell, fuel cell, gas sensor, and heterogeneous catalyst. Especially, the oxides are becoming important catalysts for the selective partial oxidation of hydrocarbons to useful products. For example, the promoted lanthanide oxides seem within the most promising catalysts in the partial oxidation of methane.[1,2] The catalytic activities of metal oxides are closely linked to their nonstoichiometric composition and electronic properties. Ambigues *et al*[3] showed that correlations between the electrical conductivity and catalytic activity exist in metal oxide. Following their investigation of the conductivity effect of adsorbed oxygen on *n*-type zinc oxide, the catalytic effect on the other *n*-type and comparative results of *p*-type metal oxides led us to search for the correlations between oxide structure and catalytic activities. It is believed that the study of electrical properties of metal oxide catalyst is essential to success in the preparation of improved catalyst. It has been reported that neodymium oxide shows a good C_2 selectivity in the catalytic methane conversion to C_2 hydrocarbons.[2] Until now, a few results have been reported for the electrical properties of neodymium oxide doped with altervalent cations. Neodymium oxide is known to be a *p*-type semiconductor, represented as $NdO_{1.5+x}$.[4,5] The electrical conductivity of neodymium oxide can be modulated by adjusting the partial pressure of oxygen at temperatures above 350℃ and its defect structure can be easily changed to oxygen vacancy by heating it with hydrogen gas. Neodymium oxide crystallizes in three different modifications: the high- temperature A- and B-modifications and the low-temperature C-modification.[6] The A-form is hexagonal La_2O_3-type lattice, the B-form is monoclinic, and the C-form is body-centered cubic. Pratap *et al*.[4] measured the electrical conductivity and dielectric constant of C-type Nd_2O_3 at 400-1100 K and found that a phase transition occurred at about 850 K. From the thermoelectric power measurements, electron hole conductivity was suggested at higher temperature. On the other hand, Dar and Lal[7] measured the electrical conductivity and dielectric constant of A-type hexagonal Nd_2O_3 pellets at 300-1200 K. They found that the conductivity is described in terms of impurity nature and space-charge polarization of thermally generated charge carrier exists above 500 K. An impurity nature was also found by Volkenkova *et al*[8] who measured the electrical conductivity of Nd_2O_3 at 500-1000℃ and Po_2 of 10^{-4} to 1 atm. Below 700℃ at $Po_2<10^{-2}$ atm, and above 800℃ at the same Po_2, the conductivity is proportional to $Po_2^{1/6}$ and $Po_2^{1/4}$, respectively.

The purpose of this work is to proceed with studies of the lower valence cation-doped neodymium oxide system. In this work, Mn-incorporated neodymium oxide systems with a variety of Mn mol% were prepared, analyzed by using XRD, XPS, SEM, DSC, and TG techniques, and their electrical conductivities were measured to investigate the effect of Mn-addition on the electrical properties of neodymium oxide in the temperature range of 500 to 1000℃ at Po_2's of 10^{-5} to 10^{-1} atm. From the results, defects and conduction

*To whom correspondence should be addressed.

mechanism in the specimen are discussed on the basis of solid-state chemistry.

Experimental

$Nd(NO_3)_3 \cdot 6H_2O$(99.9% pure, Aldrich) and $Mn(NO_3)_2$ (99.9% pure, Aldrich) were used for the preparation of Mn-incorporated neodymium oxides. The $Nd(NO_3)_3 \cdot 6H_2O$ and $Mn(NO_3)_2$ were weighed to give Nd_2O_3 containing 2, 5, 8, and 10 mol% Mn, each dissolved in deionized water, then the solutions were mixed. The resulting solutions were heated at 120℃ with continuous stirring to evaporate water, dried, calcined at 1100℃ for 96 hrs in an alumina crucible, and then slowly cooled to room temperature at a rate of 50℃/hr. X-ray powder diffractometry (XRD) for the samples was carried out using Philips PW1710 base diffractometer with CuKα as a light source and graphite monochromator in 2θ range of 20-80° to investigate the crystal structure, lattice parameters, and unit cell volumes. X-ray photoelectron spectroscopy (XPS) analyses of the specimens were performed in a PE 5000 ESCA unit to investigate the binding energy of Mn(2*p*). SEM (JCXA SP-773, JEOL) was used to investigate the grain size. To get the information of phase change in the specimens, differential scanning calorimetry (Scanton Redcraft) and thermogravimetry (PTC-10A, Rigaku) analyses were performed at a heating rate of 5℃/min in air.

The dc conductivity was measured by means of the four-contact method[9] in the temperature range of 500 to 1000℃ at Po_2's of 10^{-5} to 10^{-1} atm. To measure the electrical conductivity, the powdered samples were made into pellets under a pressure of 100 MPa under vacuum at room temperature. The pellets were sintered in air at 1100℃ for 96 hrs, annealed at 1000℃ for 48 hrs, and then quenched to room temperature. After sintering, the sample was given a light abrasive polish on one surface, and then turned over and polished until the voids on both face of the specimen were fully eliminated. The sample was then cut into a rectangular shape with dimensions of 1.2×0.6×0.2 cm and polished again. Before the sample was inserted into the sample container, it was etched in dilute nitric acid solution, washed with deionized water, dried, and then connected to the Pt probes. Samples were heated in a resistance-heated tubular furnace and temperatures were controlled to within ± 2.0℃. The conductivity was measured with increasing temperature at intervals of 25℃ and each measurement was made after the conductivity reached equilibrium.

Results

Figure 1 shows schematic X-ray diffraction (XRD) patterns of pure Nd_2O_3 and Mn-incorporated Nd_2O_3 systems calcined at 1000℃. Precision parameters of the present specimens were obtained for the single-phase hexagonal structure by the Nelson-Riley method. Figure 2 shows the plots of the lattice parameters (*a* and *c*) *vs* Nelson-Riley function, $F(\theta) = 0.5\{(\cos^2\theta/\sin\theta) + (\cos^2\theta/\theta)\}$, for pure Nd_2O_3 and 5 mol% Mn-incorporated Nd_2O_3 system. The *a*-value was obtained from the *y*-axis intercept of the plot and the *c*-value was determined from the *a*-value and extrapolation of the function with $1 \neq 0$. The lattice parameters and unit cell volumes obtained for the specimens are listed in Table 1. The lattice para-

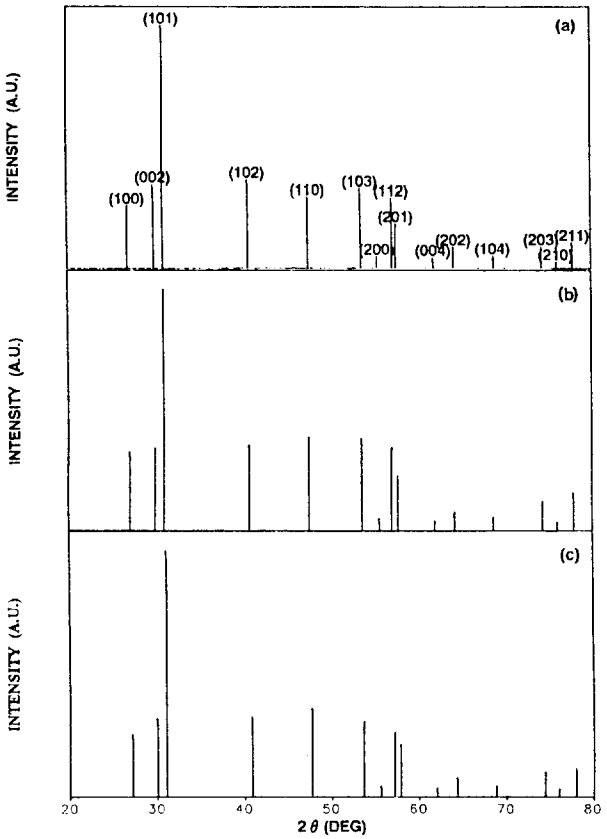

Figure 1. X-ray powder diffraction patterns of (a) pure, (b) 5 mol%, and (c) 10 mol% Mn-incorporated Nd_2O_3.

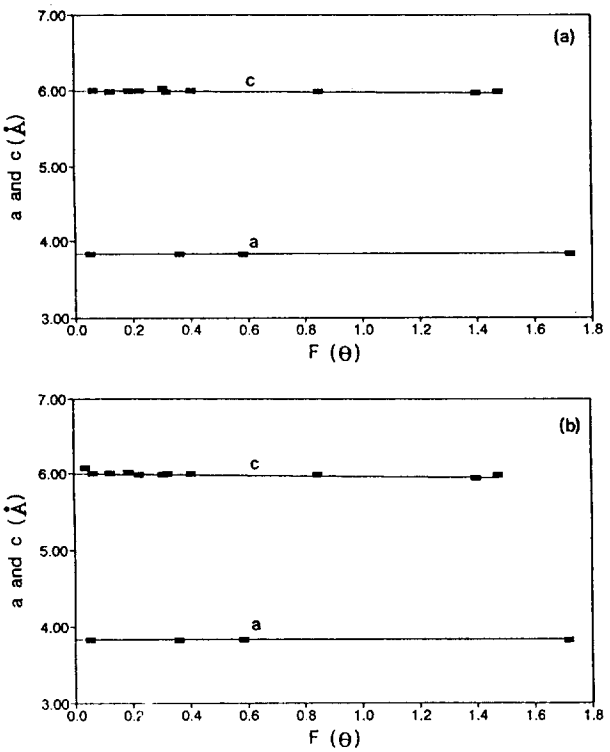

Figure 2. Plots of the lattice parameters *vs* Nelson-Riley function for (a) pure and (b) 5 mol% Mn-doped Nd_2O_3.

Table 1. Lattice parameters and unit cell volumes for pure and Mn-incorporated Nd_2O_3 systems

Mn mol%	a (Å)	c (Å)	V (Å^3)
0	3.828	6.016	76.36
2	3.827	6.009	76.22
5	3.826	5.998	76.03
8	3.825	5.991	75.93
10	3.823	5.977	75.64
12	3.821	5.941	75.10

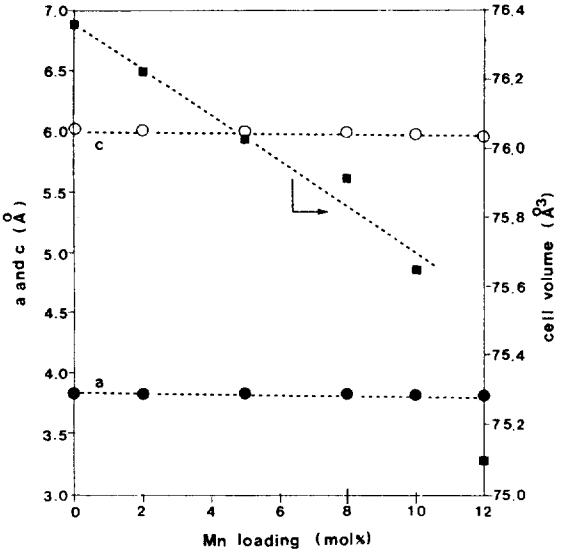

Figure 3. Lattice parameters (a and c) and cell volumes determined by Nelson-Riley function for the various Mn-incorporated Nd_2O_3 systems.

meters for pure Nd_2O_3 are $a=3.828$ and $c=6.016$ Å and the values are reasonably agreed with the values, $a=3.831$ and $c=5.999$ Å, listed in ASTM. Figure 3 shows a plot of lattice parameters *vs* dopant Mn mol%, in which a good linearity with increasing dopant mol% is observed. The linear decrease in the lattice parameters for the hexagonal phase of Mn-incorporated Nd_2O_3 is in agreement with Vegard's law expected for a true solid solution. The result indicates that the present specimens form complete solid solutions with Mn doping up to 10 mol% and their stable crystalline phases are hexagonal. The decrease in lattice parameters with increasing Mn mol% can be explained by the fact that the ionic radius of Mn^{2+} (0.80 Å) is smaller than that of Nd^{3+} (1.08 Å).

The scanning electron photomicrographs in Figure 4 show that the grain size in 10 mol% Mn-incorporated Nd_2O_3 is smaller than that in pure Nd_2O_3. From the results of SEM analyses, it is believed that relatively volatile manganese oxide inhibits the growth of grain in the system. DSC analyses showed no phase transition in the specimens in the temperature range of 25 to 900℃. Figure 5 shows the curves of DSC and TG for pure and 10 mol% Mn-incorporated Nd_2O_3, in which mass change in 10 mol% Mn-incorporated Nd_2O_3 is somewhat larger than that in pure Nd_2O_3, implying the

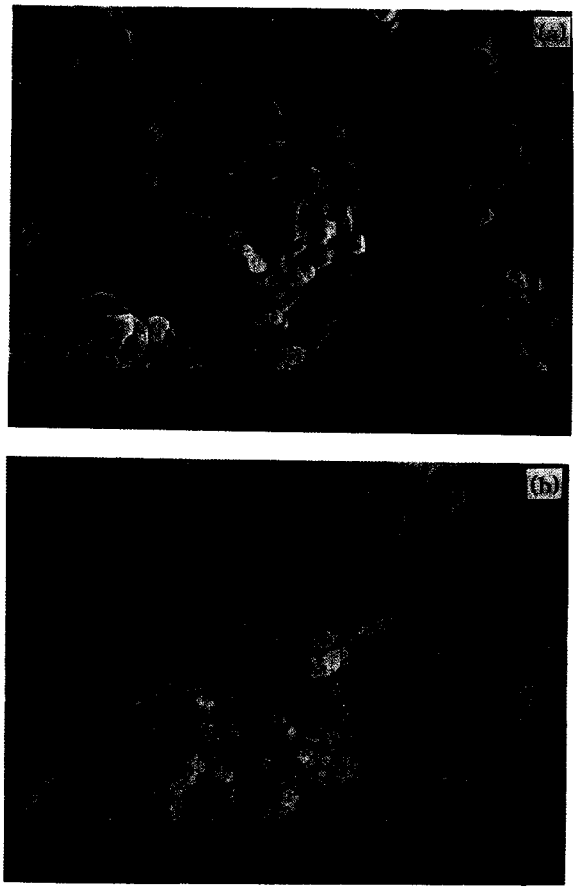

Figure 4. Scanning electron photomicrographs of (a) pure and (b) 10 mol% Mn-incorporated Nd_2O_3.

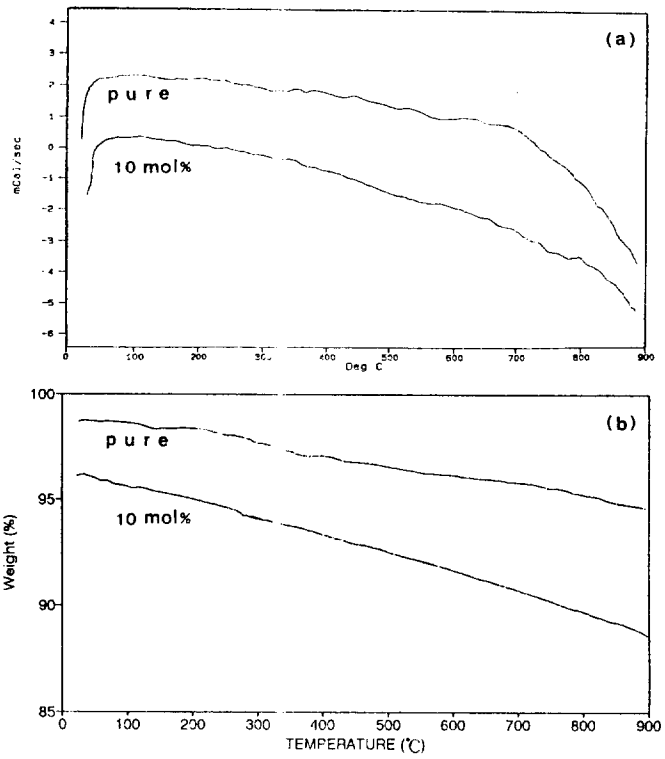

Figure 5. (a) DSC and (b) TGA curves of pure and 10 mol% Mn-incorporated Nd_2O_3.

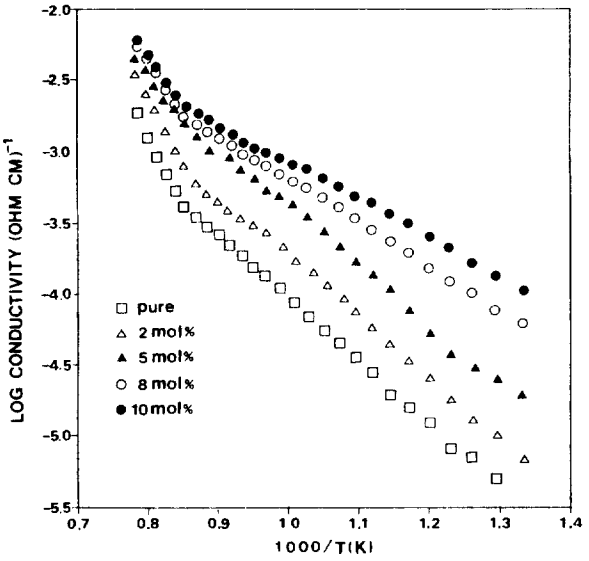

Figure 6. Plot of the log conductivity *vs* 1000/T at $Po_2=2\times10^{-1}$ atm for Mn-incorporated Nd_2O_3 systems.

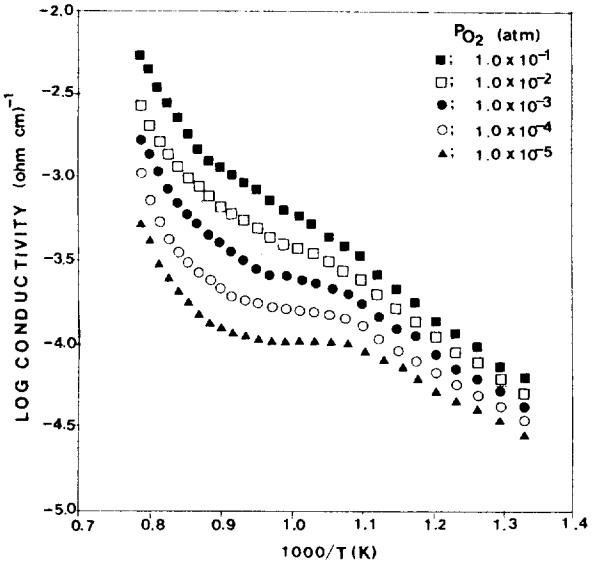

Figure 7. Plot of log conductivity *vs* 1000/T at various oxygen partial pressures for 8 mol% Mn-incorporated Nd_2O_3.

Table 2. Activation energies of pure Nd_2O_3 and Mn-incorporated Nd_2O_3 systems at $Po_2=2\times10^{-1}$ atm in the high- and low-temperature regions

Mn loading (mol%)	Activation Energy (eV)	
	Low-Temp. Region (500-850℃)	High-Temp. Region (850-1000℃)
0	0.87	1.91
2	0.87	1.89
5	0.85	1.80
8	0.64	1.45
10	0.53	1.40

elimination of manganese from the surface at high temperatures. XPS analyses showed that the binding energies of Mn ($2p_{3/2}$) for 5 mol% and 10 mol% Mn-doped Nd_2O_3 quenched from 600℃ to room temperature in air were 639.7 eV and 639.2 eV, respectively. Although broad Mn($2p_{3/2}$) peaks having FWHM of 2.70-2.85 eV were obtained, the binding energies were close to the 640.6 eV for MnO reported by Oku *et al.*[10]

Figure 6 shows a temperature dependence of electrical conductivity plotted as a function of reciprocal of absolute temperature for pure Nd_2O_3 and various Mn-incorporated Nd_2O_3 systems in the temperature range from 500 to 1000℃ at Po_2 of 2×10^{-1} atm. The electrical conductivity increases with increasing temperature and the concentration of Mn dopant. The curves are divided into high- and low-temperature regions with inflection points near 820-890℃. Activation energy for each sample was calculated from the conductivity-temperature data and the values are listed in Table 2. The activation energies fall into two regions of low and high temperatures. The significant difference in the activation energies for the the high- and low-temperature region implies that electrical conduction mechnism varies with temperature.

The electrical conductivities of the present specimens were increased with increasing temperature and Po_2. Figure 7 shows isobaric conductivity plotted against 1/T for the 8 mol% Mn-doped Nd_2O_3 system, in which the electrical conductivity increases with increasing temperature and oxygen partial pressure, indicating the specimen to be a *p*-type semiconductor.

Discussion

Figure 7 shows log conductivity *vs* 1/T for 8 mol% Mn-incorporated Nd_2O_3 at various oxygen partial pressures from 10^{-5} to 10^{-1} atm and temperatures from 500 to 1000℃. At Po_2's below 10^{-3} atm, the electrical conductivity slowly increases with increasing temperature up to 660℃, is nearly constant in the range of 660 to 850℃, and then steeply increases above 850℃. Pure Nd_2O_3 did not show the behavior. The curve shapes obtained at Po_2's above 10^{-2} atm are different from those at Po_2's below 10^{-3} atm. Namely, the curves at low oxygen partial pressures are divided into three regions, but the curves at high oxygen partial pressures are divide into two regions of high- and low-temperature. The behavior is unusal in metal oxides. As shown in Figure 5, DSC anaysis showed that phase changes of the specimens did not occur in the temperature range from 25 to 900℃. It has been known that the phase transition of neodymium oxide is mainly dependent on temperature rather than oxygen pressure.[6] Therefore, the result of Figure 7 enables us to consider that oxygen-surface interaction on Nd_2O_3 is the main cause of the change in the electrical conductivity. The oxygen chemisorption on the surface of the oxide brings about a decrease of electrical conductivity, whreas the oxygen incorporation into the oxide brings about an increase of electrical conductivity. These processes can be explained as follows. Neodymium sesquioxide has been known to be an excess oxygen metal oxide. In the case of excess oxygen metal oxide, the predominant defects may be metal vacancies or interstitial oxygen atoms.[11] Excess oxygens in metal oxide

can exist in the form of interstitial oxygen atoms or ions. The neutral interstitial oxygen atoms may in principle be ionized to yield electron holes and oxygen ions with negative effective charges and then, a *p*-type conductivity of the oxide can be observed. When Mn^{2+} ions are doped into Nd_2O_3, oxygen vacancies can be generated as charge-compensating defects and the defect equation may be written as

$$Mn_{Mn}+O_o^x=Mn'_{Nd}+O_o^x+1/2\ V\ddot{o} \quad (1)$$

where Mn'_{Nd} is effectively singly ionized manganese doped into a Nd ion site and Mn^{2+} ions act as electron hole donor. It is well known that the oxygen vacancy($V\ddot{o}$-$2\acute{e}$) can act as an adsorption site for oxygen molecule. When O_2 is adsorbed on the surface, the electron concentration should decrease according to the equilibrium (2) and the electrical conductivity accordingly decreases.

$$O_2(g)+2e'=2O^-(ads) \quad (2)$$

where e' is a conduction electron trapped at an oxygen vacancy.

In this work, the present specimens were found to be *p*-type semiconductors and the electrical conductivitiy increased with increasing Mn mol%. The results indicate that the concentration of electron hole increases with Mn doping. As listed in Table 2, the activation energies in the high-temperature region are very larger than those in the low-temperature region, which means that the energy for the formation of electronic defects is needed at higher temperatures. From the interaction between oxygen molecules and oxygen vacancies in the oxide, electron holes can be generated by the equilibrium (3) and then, the specimen has a *p*-type character.

$$V\ddot{o}+1/2\ O_2(g)=O_o^x+2\ \dot{h} \quad (3)$$

Eq. (3) means that oxygen molecule is incorporated into the lattice under high partial pressure of oxygen. Charge carriers are dissipated by Eq. (2), whereas created by Eq. (3). If the O_2-chemisorption process by Eq. (2) is more predominant than the diffusion process of oxygen by Eq. (3), a slow-increasing of electrical conductivity with temperature will be observed as shown in Figure 7. When the oxygen incorporation into the oxide becomes predominant, the electrical conductivity will be steeply increased again. Consequently, it is believed that the electrical conductivity of Mn-incorporated Nd_2O_3 is influenced by the oxygen chemisorption in the range from 660 to 850℃ at Po_2's below 10^{-3} atm and the chemisorption effect diminishes at Po_2's above 10^{-2} atm.

At temperatures above 850℃, it is suggested that the electrical conductivity depends on the change in the extent of nonstoichiometry of the oxide: the incorporation into or extraction of oxygen from the oxide. Since the electrical conductivity increases with increasing Mn mol%, Eq. (1) and (3) should contribute to the electrical conduction at high temperatures. We can derive the Po_2 dependence of electrical conductivity at high temperatures from Eq. (3). By applying the law of mass action to Eq. (3)[12], we obtain the equilibrium constant $K_3(T)$

$$K_3(T)=[O_o^X][\dot{h}]^2[V\ddot{o}]^{-1}Po_2^{-1/2} \quad (4)$$

Assuming that approximately $[O_o^x]\simeq 1$,

Table 3. Temperature dependence of the $1/n$ values in $\sigma \propto Po_2^{1/n}$ for Mn-doped Nd_2O_3 systems

Mn mol%	Temp. (℃)			
	500	600	900	1000
2	0.120	0.122	0.243	0.238
5	0.110	0.124	0.246	0.234
8	0.085	0.126	0.245	0.240

$$p^2\simeq[V\ddot{o}]Po_2^{1/2}K_3(T) \quad (5)$$

where p is electron hole concentration. The condition for electroneutrality gives $[V\ddot{o}]+2p=2[Mn'_{Nd}]$. However, $[V\ddot{o}] \gg p$, therefore $[V\ddot{o}]\simeq 2[Mn'_{Nd}]$, and Eq. (5) becomes

$$p\simeq\{K_3(T)2[Mn'_{Nd}]\}^{1/2}Po_2^{1/4} \quad (6)$$

Thus the concentration of electron holes is proportinal to $Po_2^{1/4}$ at high oxygen pressures. Since the electrical conductivity (σ) is proportinal to electron hole concentration, the electrical conductivity should be dependent on $Po_2^{1/4}$. As shown in Table 3, the Po_2 dependence of electrical conductivity measured at 900℃ is 0.243-0.245. The experimentally observed values are close to the predicted value, 0.25. Therefore, it is believed that the electrical conduction is carried by the electron hole generated by Eq. (3). Namely, at high temperatures electron hole is created by the reaction of oxygen with oxygen vacancy. On the other hand, as was mentioned already, metal vacancies are also considered as alternative predominant defects in Nd_2O_3. When oxygen is incorporated into Nd_2O_3, the formation of metal vacancies is possible. The metal vavancy (V_M^X) can be ionized to triply charged vacancies, resulted in the increase of electron hole concentration, and the disorder reaction may be written as

$$3/4\ O_2(g)=3/2\ O_o^X+V_{Nd}'''+3\ \dot{h} \quad (7)$$

If predominant defects in Nd_2O_3 are charged metal vacancies, substitutional dissolution of Mn^{2+} ions can reduce the concentration of metal vacancy and the equation can then be written as

$$Mn_{Mn}+O_O^X+V_{Nd}^X=Mn_{Nd}'+\dot{h}+O_O^X \quad (8)$$

Eq. (8) indicates that the concentration of electron hole is decreased by Mn doping. Therefore, if metal vacancies are predominant defects, the electrical conductivity of Nd_2O_3 should be decreased with increasing Mn mol%. This is not consistent with the result obtained in this work. Consequently, metal vacancies are not predominant in Nd_2O_3.

In the low-temperature region below 850℃, the activation energies obtained are 0.85-0.87 eV for lightly doped Nd_2O_3 systems containing Mn below 5 mol% and 0.53-0.64 eV for highly doped Nd_2O_3 systems containing Mn above 8 mol% as listed in Table 2. The activation energies (0.85-0.87 eV) of lightly doped specimens are close to 0.87 eV of pure Nd_2O_3, but the activation energy (0.53 eV) of 10 mol% Mn-doped Nd_2O_3 is lower than the value of pure Nd_2O_3. This result can be explained on the basis that the defect formation is facilitated by the addition of Mn impurity and the carriers may be saturated in the donor sites. Moreover, it can't also

be excluded that in highly doped specimens a composition exerts a effect on the coulombic interactions of the free Mn'Nd dopant ions and the charged associates $\{Mn'_{Nd}V\ddot{o}\}^{\cdot}$, and the activation energy can then be varied. The Po_2 dependence (0.08-0.13) of electrical conductivity at 500 and 600℃ enable us to consider the possibility of a mixed conduction. Volkenkova *et al*[8] measured the electrical conductivity of Nd_2O_3 at 500-1000℃ and Po_2 of 10^{-4} to 1 atm. They observed that the conductivity was proportinal to $Po_2^{1/6}$ at temperatures below 700℃ and explained the Po_2 dependence by the oxygen interstitial model. In case of oxygen interstitials being the predominant defect at low temperatures, the oxygen partial pressure dependence of the conductivity can be derived from the equilibrium between interstitial oxygen ions and gaseous oxygen and this can be expressed by

$$O_i'' + 2\,\dot{h} = 1/2\ O_2(g) \tag{9}$$

In this case, the interstitial oxygen ion is considered to become fully ionized. From the equilibrium (9), we can get

$$[\dot{h}] = (1/K_9[O_i''])^{1/2}\ Po_2^{1/4} \tag{10}$$

For large excess of oxygen, that is, when $[O_i''] = 1/2\ [\dot{h}] \gg [V\ddot{o}]$ the following relation is obtained.

$$p = K\ Po_2^{1/6},\ K = (2/K_9)^{1/2}. \tag{11}$$

Therefore, if interstitial oxygens are predominant in the oxide, the electrical conductivity will be proportinal to $Po_2^{1/6}$. The amount of excess oxygen in Nd_2O_3 decreases with increasing temperature.[5] At high temperatures above 800℃, oxygen vacancies are formed in the oxide and then, electron holes can be generated from the interaction between oxygen molecules and oxygen vacancies, resulted in $\sigma \propto Po_2^{1/4}$.

In this work, the electrical conductivity data measured as a function of Po_2 at 500 and 600℃ for Mn-doped Nd_2O_3 systems were not fitted to $\sigma \propto Po_2^{1/6}$. As listed in Table 3, the Po_2 dependences of electrical conductivity for Mn-doped Nd_2O_3 systems are 0.085-0.120 at 500℃ and 0.122-0.126 at 600℃, which implies that the electrical conduction is not carried by only electron hole and may include an ionic conductivity at low temperatures. If the electron hole conductivity is coupled with an ionic conductivity which is independent of the Po_2, the oxygen pressure dependence on electrical conductivity should decrease. According to the report of Berard *et al*[13], the activation energy for the diffusion of cation in lanthanide oxide is larger than that of anion and the movement of oxygen ions through the ⟨111⟩ open pathway is promoted. Eyring *et al*[14] also reported on the diffusion of lanthanide oxides that the movement of oxygen is possible even at the low temperature of 400℃, but no mobile cations are observed even at the high temperature of 1200℃. Based on these reports, Mn-doped Nd_2O_3 systems may include ionic conduction owing to the diffusion of oxygen atoms through ⟨111⟩ open pathways in the lower temperature region. The Po_2 dependence of electrical conductivity measured at 500℃ decreased with increasing the amount of Mn-dopant as shown in Table 3, which implies that the ionic conduction in Mn-doped Nd_2O_3 increases with the Mn mol%. The ionic conductivity of metal oxide can be increased by the diffusion of oxygen atoms. The present systems are expected to contain oxygen vacancies and thus, the diffusion of oxygen is promoted. As a result of ionic diffusion, an increase in ionic conductivity may be expected and the conductivity is unaffected by the oxygen partial pressure in the lower temperature region. Consequently, it is expected that there are many oxygen vacancies in highly Mn-doped Nd_2O_3 system and thus, the diffusion of oxygen is promoted.

Acknowledgement. The present study was supported by the Basic Science Research Institute Program (No. BSRI-91-330), Ministry of Education of Korea, 1991.

References

1. Campbell, K. D.; Zhang, H.; Lunsford, J. H. *J. Phys. Chem.* **1988**, *92*, 750.
2. Feng, Y.; Niiranen, J.; Gutman, D. *J. Phys. Chem.* **1991**, *95*, 6558.
3. Ambiques, P.; Teichner, S. J. *Discuss Faraday Soc.* **1966**, *41*, 362.
4. Pratap, V.; Verma, B. K.; Lal, H. B. *Proc. Natl. Acad. Sci., India Sect.* **1978**, *A48*, 20.
5. Barrett, M. F.; Barry, T. I. *J. Inorg. Nucl. Chem.* **1965**, *27*, 1483.
6. Hyde, B. G.; Eyring, L. In *Rare earth research III*; Eyring, L., Ed.; Gordon & Breach Sci. Pub. Inc.: New York, U. S. A., 1962; p 339.
7. Dar, N.; Lal, H. B. *Pramana*, **1976**, *7*, 245.
8. Volkenkova, Z. S.; Chebotin, V. N. *Izv. Akad. Nauk. SSSR, Neorg. Matter*, **1974**, *10*, 1275.
9. Runyan, W. R. In *Semiconductor measurements and instrumentation*; McGraw-Hill Co.: New York, U. S. A., 1975; p 65.
10. Oku, M.; Hirokawa, K.; Ikeda, S. *J. Elect. Spect. Relat. Phenomena*, **1975**, *7*, 465.
11. Rao, G. V. S.; Ramdas, S.; Mehrotra, P. N.; Rao, C. N. R. *J. Sol. State Chem.* **1970**, *2*, 377.
12. Kilner, J. A.; Steele, B. C. H. In *Mass transport in anion-deficient fluorite oxides*; Sorenson, O. T. Ed.; Academic Press: New York, U. S. A., 1981; p 233.
13. Berard, M. F.; Wilder, D. R. *J. Am. Cer. Soc.* **1969**, *52*, 85.
14. Eyring, L.; Holmberg, B. In *Nomstoichiometric compounds*; Am. Chem. Soc.: Washington D. C., U. S. A., 1963; p 46.